

Solution of the Linear Hyperbolic Heat Equation using the Finite Element Method

Kim R. Kristiansen, Ludwig Lahmeyer^a

^a*Norges teknisk-naturvitenskapelige universitet, 7491 Trondheim, Norway*

Abstract

The linear hyperbolic heat equation, describing hyperbolic heat conduction under certain assumptions of isotropy, was solved on a 1-dimensional interval, 2-dimensional square, and a 3-dimensional cube, using the finite element method. The solution was approximated by projection onto finite subspaces consisting of piecewise linear and piecewise quadratic polynomials. The resulting semi-discretized system was solved using the backward Euler method, and the problems were solved using a variety of Dirichlet and Neumann boundary conditions. Emphasis was put on illustrating the differences in qualitative behaviour of the standard heat equation and the hyperbolic variant, and their implications for physical heat transfer on short time scales.

1. General Theory

In this project, we consider a generalized version of the heat equation for an isotropic system, with an added inertia term such that the heat propagation is characterized by a characteristic relaxation time τ . The starting point for all variations of the problem is the Cattaneo-Vernotte equation for the heat flux \mathbf{J}_q

$$\mathbf{J}_q = -\lambda \nabla T - \tau \partial_t \mathbf{J}_q \quad (1)$$

along with conservation of energy

$$\partial_t (c_v T) + \nabla \cdot \mathbf{J}_q = 0 \quad (2)$$

where λ is the thermal conductivity, c_v the heat capacity, and T the temperature. Assuming that the heat capacity is not explicitly time-dependent, and that the relaxation time remains constant throughout the system, combining the two equations yields

$$\partial_t T = c_v^{-1} \nabla \lambda \cdot \nabla T + D \nabla^2 T - \tau \partial_t^2 T \quad (3)$$

where $D = \lambda/c_v$ is the thermal diffusivity. In an otherwise isotropic system, the gradient in thermal conductivity will arise due to the temperature gradients in the system. We can rewrite the first term on the right hand side as

$$c_v^{-1} \nabla \lambda \cdot \nabla T = c_v^{-1} \partial_T \lambda (\nabla T)^2 \quad (4)$$

which will act as a nonlinear advection term. Neglecting the temperature dependence of λ yields a simpler linear equation

$$\partial_t T + \tau \partial_t^2 T = D \nabla^2 T \quad (5)$$

which can be recognized as the classical heat equation, modified with an additional term $\tau \partial_t^2 T$. The effect of this term is that it limits the speed at which information about a temperature perturbation travels through the system. A relativistic treatment of heat conduction will necessarily produce such a term such that the speed of information is bounded above by the speed limit of causality. Solutions to the classical

heat equation, on the other hand, will change instantaneously on the entire domain, if ever so slightly. It is therefore interesting to investigate how the solutions to these two equations differ when the time scales are short compared to the length scales in the system. For boundary conditions, two different types will be explored. We divide the boundary such that $\partial\Omega = \Gamma_D \cup \Gamma_N$. Γ_D will be thermostatted (i.e. kept at a constant temperature), and Γ_N will be thermally insulated, which means that the heat flux normal to the boundary vanishes. We will focus on the linear equation (5), such that the complete problem statement is: find T satisfying

$$\begin{aligned} \partial_t T + \tau \partial_t^2 T &= D \nabla^2 T && \text{on } \Omega \\ T = T_\partial && \text{on } \Gamma_D & \quad \nabla T \cdot \mathbf{n} = 0 && \text{on } \Gamma_N \end{aligned} \quad (6)$$

where T_∂ contains the temperatures on Γ_D , and the Neumann condition on Γ_N comes from the fact that we demand that $\mathbf{J}_q \cdot \mathbf{n} = 0$ on Γ_N for all times t , such that we also have $\partial_t \mathbf{J}_q \cdot \mathbf{n} = 0$, which leaves $\lambda \nabla T \cdot \mathbf{n} = 0$ by (1). Consider a modification of the above problem where $T_\partial = 0$, and denote by V the Hilbert space containing the solution \dot{T} for the homogeneous problem. Let v be an arbitrary function from this space, and consider the projection of (5) onto v . We obtain

$$\int_{\Omega} v \partial_t T \, d\mathbf{r} + \tau \int_{\Omega} v \partial_t^2 T \, d\mathbf{r} = D \int_{\Omega} v \nabla^2 T \, d\mathbf{r} = D \int_{\partial\Omega} v \nabla T \cdot \mathbf{n} \, dS - D \int_{\Omega} \nabla v \cdot \nabla T \, d\mathbf{r} \quad (7)$$

We have that the surface integral over $\partial\Omega$ on the right hand side must vanish, because $\nabla T \cdot \mathbf{n} = 0$ on Γ_N , and that $v = 0$ on Γ_D as it is an arbitrary function from the space of functions satisfying the homogeneous Dirichlet conditions. Lifting the boundary conditions such that $T \rightarrow T + T_\partial$, the left hand side does not change because T_∂ is by assumption time-independent. The final weak formulation of the problem is: find T such that

$$\int_{\Omega} v \partial_t T \, d\mathbf{r} + \tau \int_{\Omega} v \partial_t^2 T \, d\mathbf{r} = -D \int_{\Omega} \nabla v \cdot \nabla T \, d\mathbf{r} - D \int_{\Omega} \nabla v \cdot \nabla T_\partial \, d\mathbf{r} \quad (8)$$

for all $v \in V$. Projecting this equation onto a finite-dimensional subspace $V_h \subset V$ with complete basis $\{\phi_i\}$, we express v and T as linear combinations of the basis functions, such that the equation becomes

$$\sum_{i,j} v_i \dot{T}_j \int_{\Omega} \phi_i \phi_j \, d\mathbf{r} + \tau \sum_{i,j} v_i \ddot{T}_j \int_{\Omega} \phi_i \phi_j \, d\mathbf{r} = -D \sum_{i,j} v_i T_j \int_{\Omega} \nabla \phi_i \cdot \nabla \phi_j \, d\mathbf{r} - D \sum_{i,j} v_i T_{\partial,j} \int_{\Omega} \nabla \phi_i \cdot \nabla \phi_j \, d\mathbf{r} \quad (9)$$

with dots indicating time derivatives. In linear algebra form, we can write this as

$$\mathbf{v}^T \mathbf{M} (\tau \ddot{\mathbf{T}} + \dot{\mathbf{T}}) = -D \mathbf{v}^T \mathbf{A} \mathbf{T} - D \mathbf{v}^T \mathbf{A} \mathbf{T}_\partial \quad (10)$$

with \mathbf{v} and \mathbf{T} being vectors containing the expansion coefficients for v and T , respectively. The stiffness matrix \mathbf{A} and mass matrix \mathbf{M} are defined component-wise as

$$A_{ij} = \int_{\Omega} \nabla \phi_i \cdot \nabla \phi_j \, d\mathbf{r} \quad M_{ij} = \int_{\Omega} \phi_i \phi_j \, d\mathbf{r} \quad (11)$$

and since (10) must hold for all \mathbf{v} , we must have that

$$\mathbf{M} (\tau \ddot{\mathbf{T}} + \dot{\mathbf{T}}) = -D \mathbf{A} \mathbf{T} - D \mathbf{A} \mathbf{T}_\partial \quad (12)$$

which is an inhomogeneous linear system of second order ODEs for the expansion coefficients of T , which can be recast into a system of first order ODEs as

$$\begin{bmatrix} \mathbf{I} & \mathbf{0} \\ \mathbf{0} & \tau \mathbf{M} \end{bmatrix} \frac{d}{dt} \begin{bmatrix} \mathbf{T} \\ \dot{\mathbf{T}} \end{bmatrix} = \begin{bmatrix} \mathbf{0} & \mathbf{I} \\ -D \mathbf{A} & -\mathbf{M} \end{bmatrix} \begin{bmatrix} \mathbf{T} \\ \dot{\mathbf{T}} \end{bmatrix} + \begin{bmatrix} \mathbf{0} \\ -D \mathbf{A} \mathbf{T}_\partial \end{bmatrix} \quad (13)$$

or, with a straightforward change of symbols

$$\mathbf{P}\dot{\mathbf{x}} = \mathbf{S}\mathbf{x} + \mathbf{b} \quad (14)$$

which can be solved using standard ODE solvers. Solving this equation for any given time yields the numerical approximation to the exact solution as the interpolant

$$T \approx \sum_i T_i \phi_i \quad (15)$$

which can, in theory, be made arbitrarily accurate by increasing the dimension of V_h and/or choosing a basis which more accurately represents the exact solution. For integration in time, the backward Euler method (i.e. backward difference approximation) was chosen for its simplicity and stability. For a time step k , the iterations for the internal part of the coefficient vector is then

$$\left(\frac{1}{k} \mathbf{P} - \mathbf{S} \right) \mathbf{x}_i = \frac{1}{k} \mathbf{P} \mathbf{x}_{i-1} + \mathbf{b} \quad (16)$$

2. Convergence

To show convergence and stability, we will approach this problem the same way as we would the ordinary parabolic problem described in [1], with the addition of an extra hyperbolic term.

$$\int_{\Omega} \frac{\partial T}{\partial t} v d\mathbf{r} + \tau \int_{\Omega} \frac{\partial^2 T}{\partial t^2} v d\mathbf{r} + a(T, v) = -a(T_{\partial}, v) \quad (17)$$

$$\begin{aligned} \alpha \|T - T_h\|_{H^1}^2 &\leq a(T - T_h, T - v_h) + a(T - T_h, v_h - T_h) \\ &\leq M \|T - T_h\|_{H^1} \|T - v_h\|_{H^1} + a(T, v_h - T_h) - a(T_h, v_h - T_h) \\ &\leq M \|T - T_h\|_{H^1} \|T - v_h\|_{H^1} - \int_{\Omega} \frac{\partial T}{\partial t} (v_h - T_h) - \tau \int_{\Omega} \frac{\partial^2 T}{\partial t^2} (v_h - T_h) \\ &\quad + \int_{\Omega} \frac{\partial T}{\partial t} (v_h - T_h) + \tau \int_{\Omega} \frac{\partial^2 T}{\partial t^2} (v_h - T_h) \\ &\leq M \|T - T_h\|_{H^1} \|T - v_h\|_{H^1} - \int_{\Omega} \frac{\partial (T - T_h)}{\partial t} (v_h - T_h) - \tau \int_{\Omega} \frac{\partial^2 (T - T_h)}{\partial t^2} (v_h - T_h) \\ &\leq M \|T - T_h\|_{H^1} \|T - v_h\|_{H^1} - \left\langle \frac{\partial (T - T_h)}{\partial t}, (v_h - T_h) \right\rangle_{L^2} - \tau \left\langle \frac{\partial^2 (T - T_h)}{\partial t^2}, (v_h - T_h) \right\rangle_{L^2} \end{aligned} \quad (18)$$

As [1] already offers an in depth explanation as to the approach used in arriving at a convergence formula for parabolic equations, we will focus on the added hyperbolic term, not present in the [1] example.

$$\begin{aligned} \tau \left\langle \frac{\partial^2 (T - T_h)}{\partial t^2}, (v_h - T_h) \right\rangle_{L^2} &= \tau \left\langle \frac{\partial^2 (T - T_h)}{\partial t^2}, (T - v_h) \right\rangle_{L^2} - \tau \left\langle \frac{\partial^2 (T - T_h)}{\partial t^2}, (T - T_h) \right\rangle_{L^2} \\ &= \tau \left\langle \frac{\partial^2 (T - T_h)}{\partial t^2}, (T - v_h) \right\rangle_{L^2} - \tau \frac{1}{2} \frac{\partial^2}{\partial t^2} \|T - T_h\|_{L^2}^2 + 2 \frac{\partial}{\partial t} \|T - T_h\|_{L^2}^2 \end{aligned} \quad (19)$$

This result is inserted back into (18), we multiply by 2 and integrate, and once again focus on the term not present in Quarteroni's example, the first term in (19):

$$\begin{aligned}
2\tau \int_0^t \left\langle \frac{\partial^2(T - T_h)}{\partial t^2}, (T - v_h) \right\rangle_{L^2} &= -2\tau \int_0^t \left\langle \frac{\partial(T - T_h)}{\partial t}, \frac{\partial(T - v_h)}{\partial t} \right\rangle_{L^2} + 2\tau \left\langle \frac{\partial(T - T_h)}{\partial t}(t), (T - v_h)(t) \right\rangle_{L^2} \\
&\quad - 2\tau \left\langle \frac{\partial(T - T_h)}{\partial t}(0), (T - v_h)(0) \right\rangle_{L^2} \\
&\leq 2\tau \int_0^t \left\| \frac{\partial(T - T_h)}{\partial t} \right\|_{L^2}^2 \left\| \frac{\partial(T - v_h)}{\partial t} \right\|_{L^2}^2 \\
&\quad + \frac{2\tau}{4} \left\| \frac{\partial(T - T_h)}{\partial t}(t) \right\|_{L^2}^2 + 2\tau \|(T - v_h)(t)\|_{L^2}^2 \\
&\quad + \tau \left\| \frac{\partial(T - T_h)}{\partial t}(0) \right\|_{L^2}^2 + \tau \|(T - v_h)(0)\|_{L^2}^2
\end{aligned} \tag{20}$$

We now add this hyperbolic part to the parabolic part as seen in [1], gather coefficients and simplify, leaving us with:

$$\begin{aligned}
&2\tau \|T - T_h\|_{L^2}^2 - 7 \int_0^t \|T - T_h\|_{L^2}^2 + 2\alpha \int_0^t \int_0^t \|T - T_h\|_{L^2}^2 \\
&\leq \frac{2M^2}{\alpha} \int_0^t \int_0^t \|T - v_h\|_{H^1}^2 \\
&\quad + 4\tau \int_0^t \int_0^t \left\| \frac{\partial(T - T_h)}{\partial t} \right\|_{L^2}^2 \left\| \frac{\partial(T - v_h)}{\partial t} \right\|_{L^2}^2 \\
&\quad + \tau \int_0^t \left\| \frac{\partial(T - T_h)}{\partial t}(t) \right\|_{L^2}^2 + (4 + 4\tau) \int_0^t \|T - v_h\|_{L^2}^2 \\
&\quad + 2\tau \int_0^t \left\| \frac{\partial(T - T_h)}{\partial t} \right\|_{L^2}^2 + (1 + 2\tau) \int_0^t \|(T - v_h)(0)\|_{L^2}^2 \\
&\quad + \int_0^t \|(T - T_h)(0)\|_{L^2}^2 \\
&\quad + 4 \int_0^t \int_0^t \|T - T_h\|_{L^2}^2 \left\| \frac{\partial(T - T_h)}{\partial t} \right\|_{L^2}^2
\end{aligned} \tag{21}$$

We bound some of the summands of the right hand side[1], apply Gronwall's Lemma and obtain:

$$\begin{aligned}
&\left(2\tau \|T - T_h\|_{L^2}^2 - 7 \int_0^t \|T - T_h\|_{L^2}^2 + 2\alpha \int_0^t \int_0^t \|T - T_h\|_{L^2}^2 \right)^{\frac{1}{2}} \\
&\leq Ch^r \left(\sqrt{N(T)} + \int_0^t \left| \frac{\partial T}{\partial t} \right|_{H^r} + \int_0^t \int_0^t \left| \frac{\partial^2 T}{\partial t^2} \right|_{H^r} \right)
\end{aligned} \tag{22}$$

Which shows that the discretization scheme converges to the exact solution as the grid is refined. For the stability and convergence of the backward Euler method, see [1].

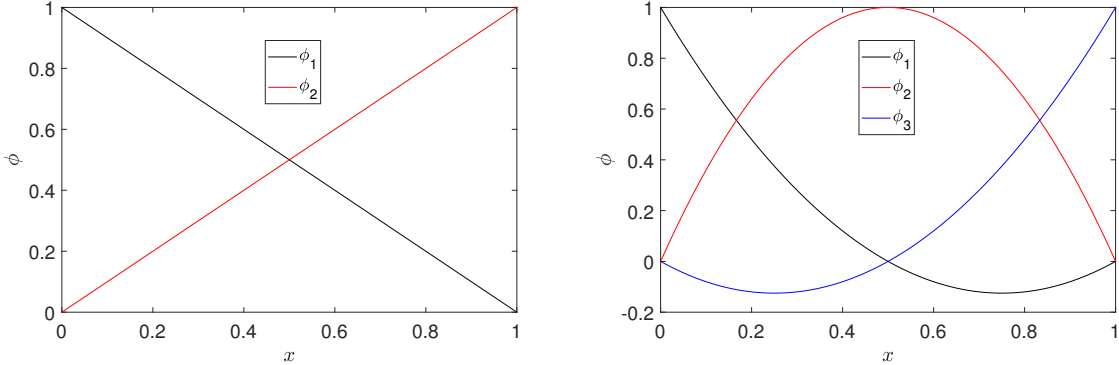


Figure 1: One-dimensional basis functions for linear elements (left) and quadratic elements (right) on the reference interval.

3. 1D Simulations

In one dimension, the triangulation of the domain is simply the partitioning into sub-intervals. The basis functions used for solving the 1D case are piecewise linear and piecewise quadratic basis functions, which are illustrated in figure 1. We consider three different cases and compare the hyperbolic equation to the conventional heat equation ($\tau = 0$):

Case 1: Both ends of the domain are thermostatted at two different temperatures, i.e. inhomogeneous Dirichlet boundary conditions, with the temperature in the interior initially equal to one of the wall temperatures. Solutions are shown in figure 2 for $D = 10^5$ and $\tau = 5 \cdot 10^8$.

Case 2: One end of the domain thermally insulated, i.e. homogeneous Neumann condition, and the other end thermostatted at a temperature different from the initial temperature in the interior. The solutions are shown in figure 3 for $D = 10^5$ and $\tau = 5 \cdot 10^8$.

Case 3: Both ends thermally insulated, with an initial non-constant temperature profile on the interior. The solutions are shown in figure 4 for a grid of 5000 internal nodes with the middle 500 nodes set to have an initial temperature of 10, and zero otherwise, with $D = 10^5$ and $\tau = 5 \cdot 10^7$.

We observe that the hyperbolic solution is more wave-like, with a wave front travelling from the high temperature wall towards the opposing wall. The wave crashes onto the wall and is reflected, illustrating that information about the other thermostat only reaches the first thermostat after a finite period of time. This type of reflection is also seen when such a wave front hits an insulated wall, where some degree of heat accumulation occurs due to the inertia of the heat flux, with a resulting backwards wave travelling back to the thermostat. For the case of a completely isolated system with an initial temperature profile, the difference between the two solutions is particularly striking. Whereas the parabolic solution simply melts down to a straight line, the hyperbolic solution splits into two wave fronts travelling in each direction and reflecting off the walls while slowly decaying.

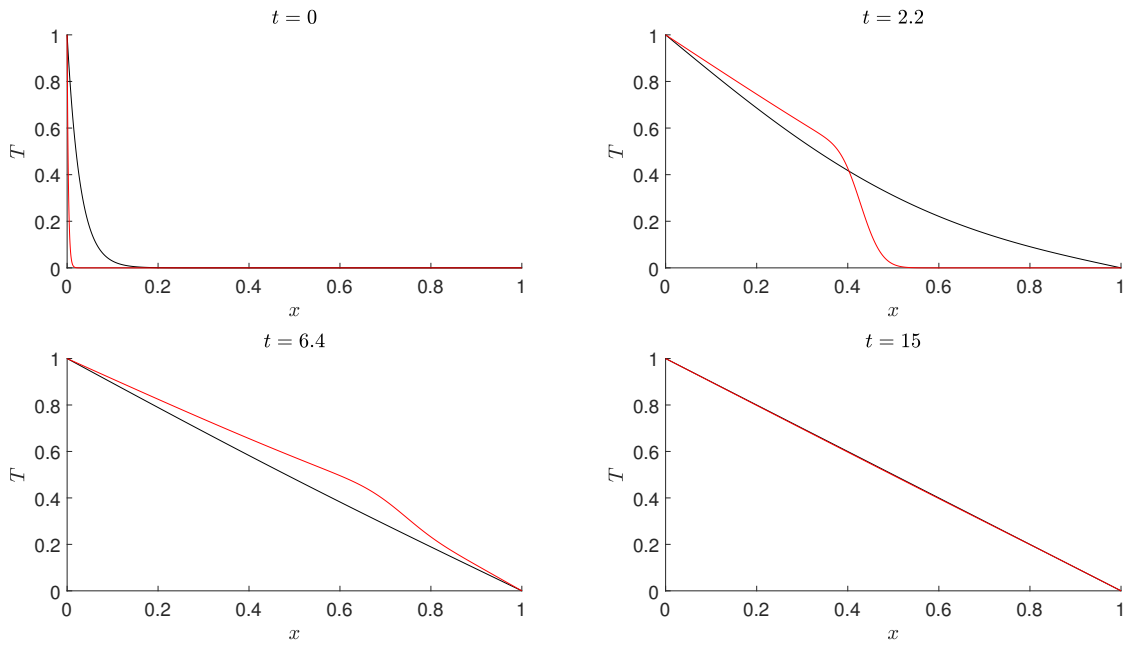


Figure 2: Snapshots of the solutions to the conventional heat equation and the hyperbolic variant with the left wall thermostatted at $T = 1$ and the right wall thermostatted at $T = 0$, with initial temperature 0 on the interior.

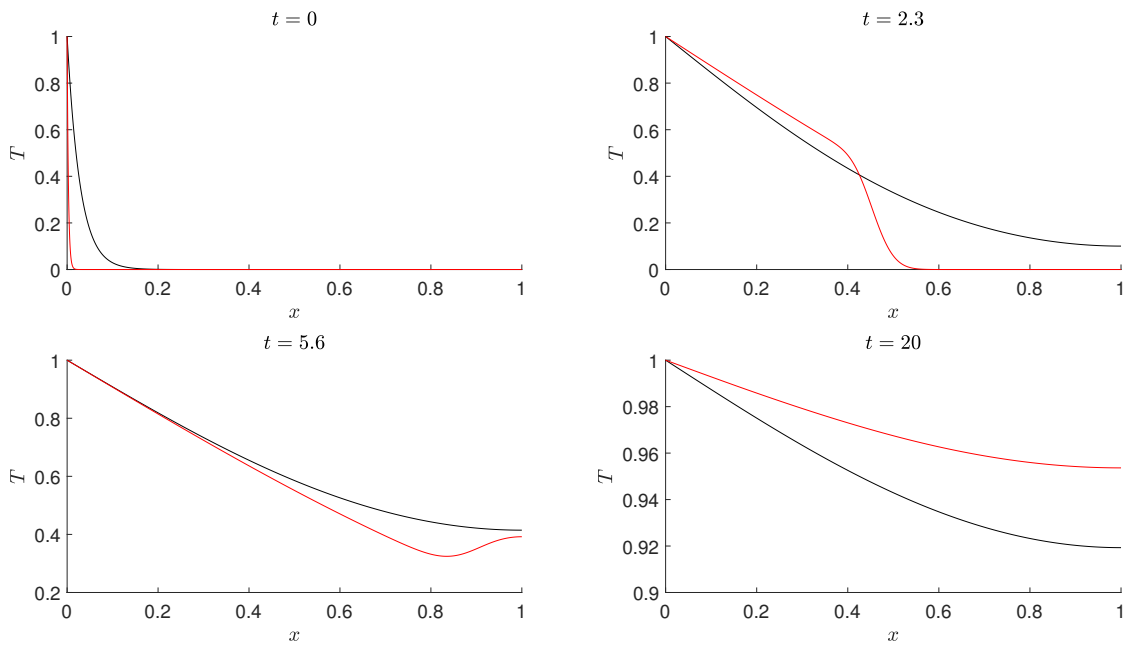


Figure 3: Snapshots of the solutions to the conventional heat equation and the hyperbolic variant with the left wall thermostatted at $T = 1$ and the right wall thermally insulated, with initial temperature zero on the interior.

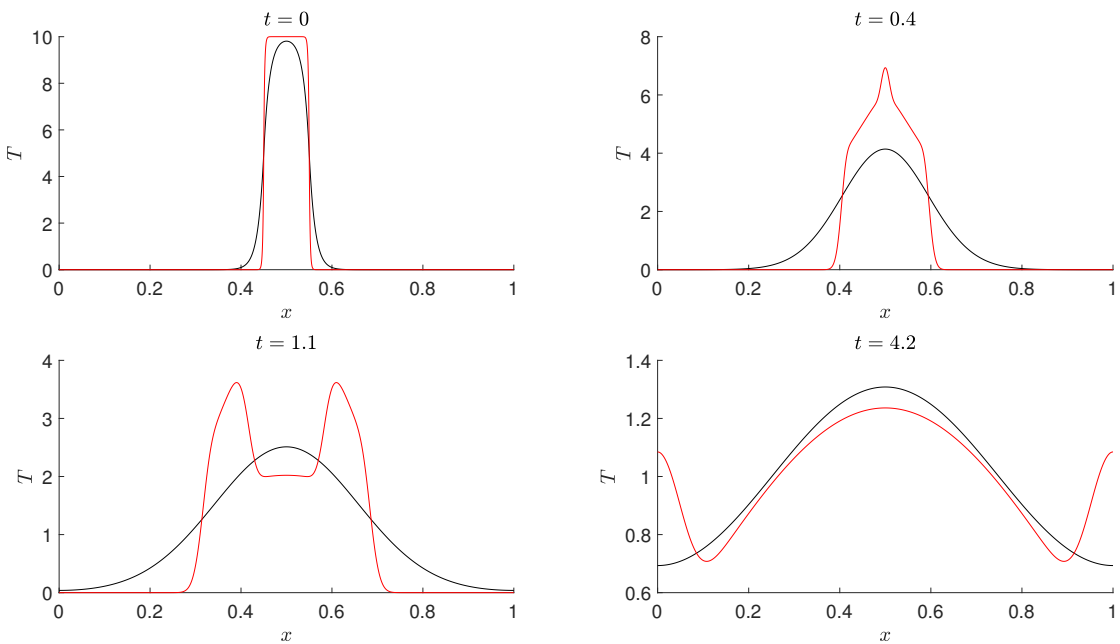


Figure 4: Snapshots of the solutions to the conventional heat equation and the hyperbolic variant with an initial temperature profile on the interior and homogeneous Neumann conditions on the boundaries.

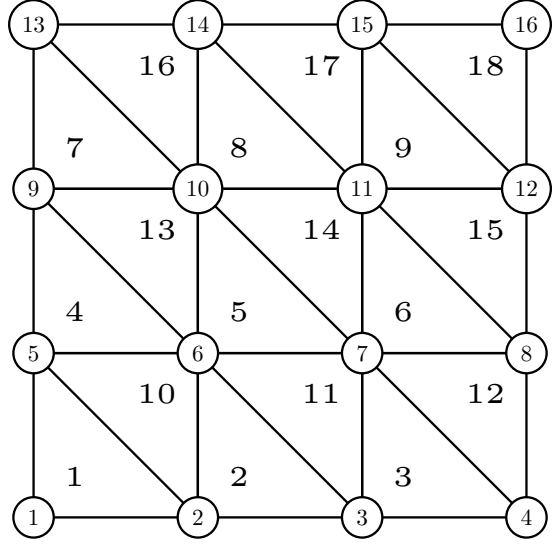


Figure 5: Triangulation of a 4×4 square grid. The 16 nodes and the 18 triangular elements are numbered in the way they are in the 2D triangulation in this project.

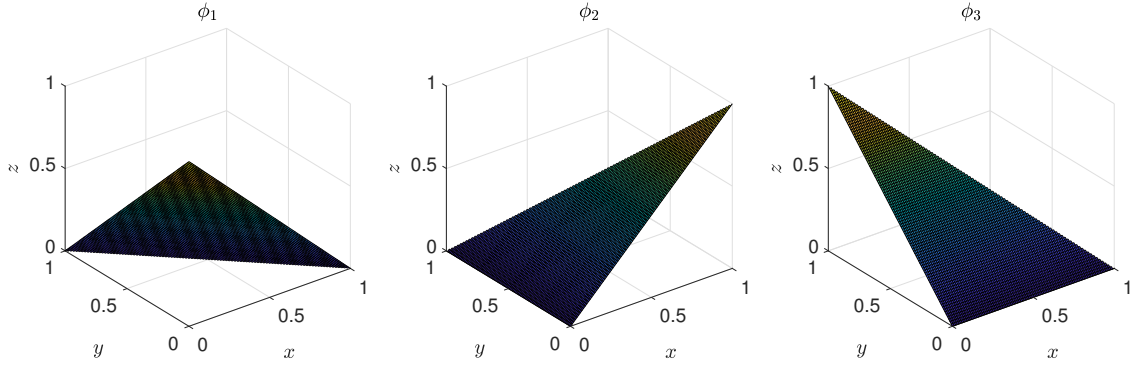


Figure 6: Two-dimensional linear basis functions on the reference triangle.

4. 2D Simulations

In two dimensions, the domain was triangulated as illustrated in figure 5. The linear and quadratic basis functions are illustrated on the reference triangle with vertices $(0, 0)$, $(0, 1)$ and $(1, 0)$ in figures 6 and 7, respectively. We consider again three different cases analogous to the 1D cases. The difference being that any walls not having a Dirichlet condition have homogeneous Neumann conditions. The case with two opposing thermostats is shown in figure 8, the case with one thermostat in figure 9, and the completely isolated system in figure 10.

In these simulations, the results are observed to be completely analogous to the one-dimensional cases. The thermostatted wall cases can briefly be described as planes of one-dimensional solutions, which is to be expected due to the translational symmetry along the y -direction for these problems. The isolated system was tested using an initial gaussian temperature profile centered at the center of the domain. Whereas the parabolic solution exhibits exactly the same type of behaviour as in one dimension, the hyperbolic solution's tendency to reflect off the walls gives some interesting effects due to the differences in symmetry properties between the initial temperature profile and the domain boundary.

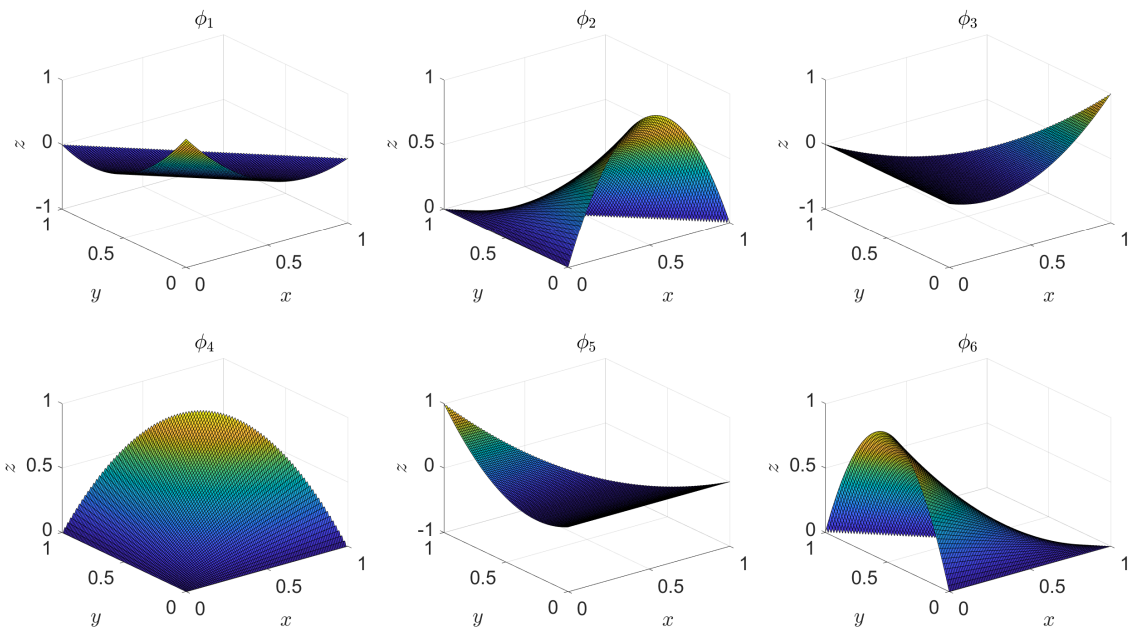


Figure 7: Two-dimensional quadratic basis functions on the reference triangle.

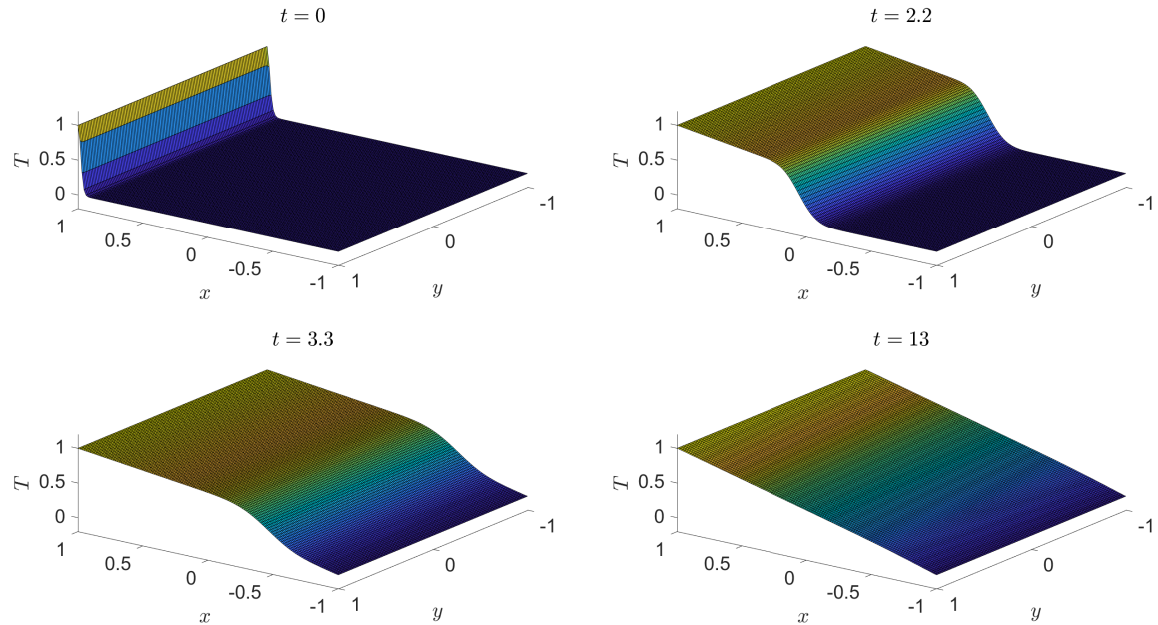


Figure 8: Snapshots of the solution to the hyperbolic heat equation in two dimensions with two opposing thermostatted walls, and the remaining walls thermally insulated.

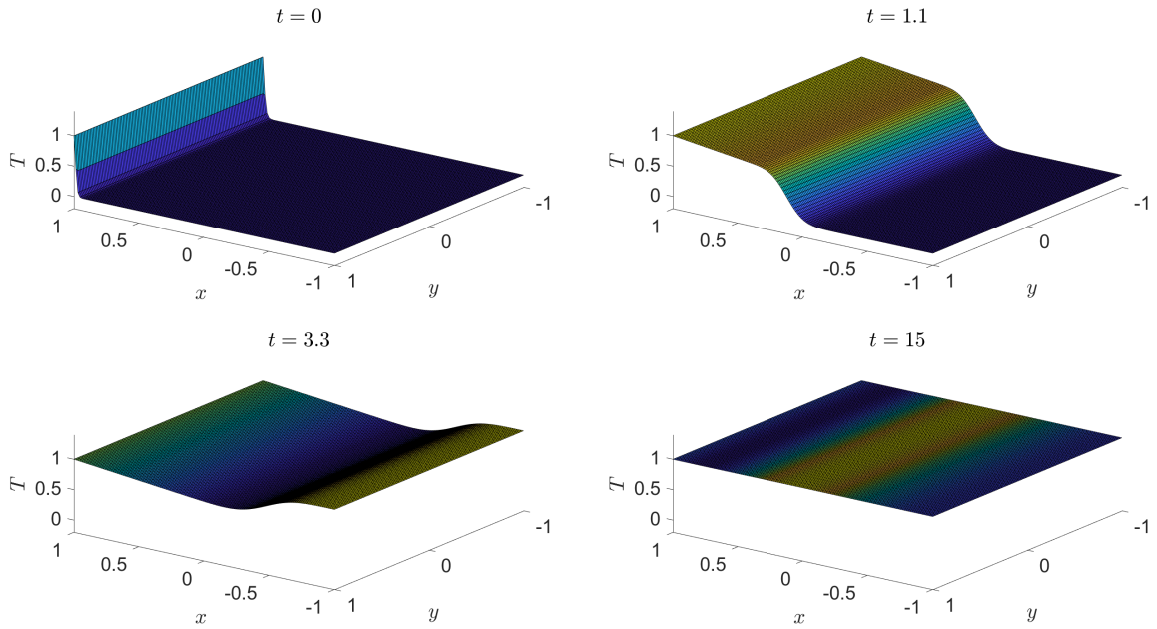


Figure 9: Snapshots of the solution to the hyperbolic heat equation in two dimensions with one thermostatted wall, and the remaining walls thermally insulated.

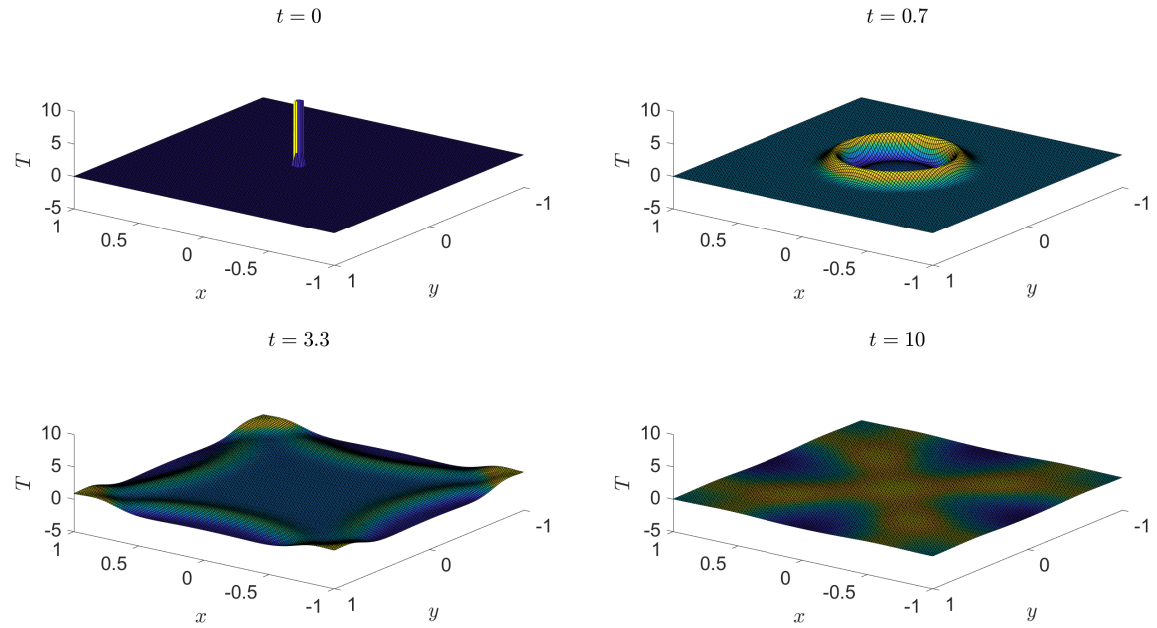


Figure 10: Snapshots of the solution to the hyperbolic heat equation in two dimensions with an initial gaussian temperature profile in the center of the interior, with all walls thermally insulated.

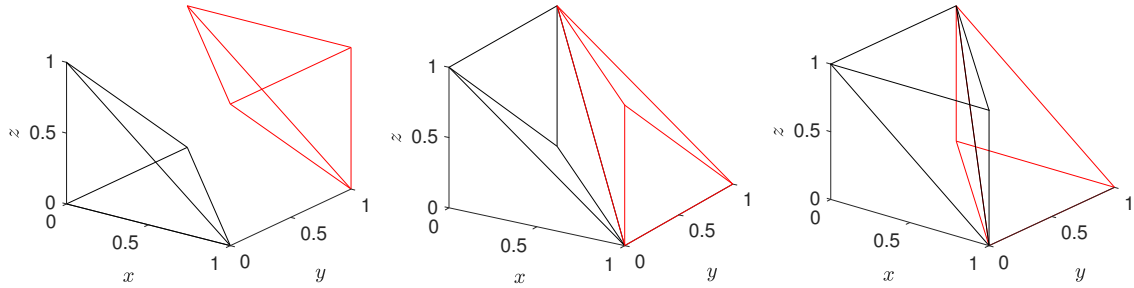


Figure 11: Illustration of the unit tetrahedra used for triangulation of the 3D domain.

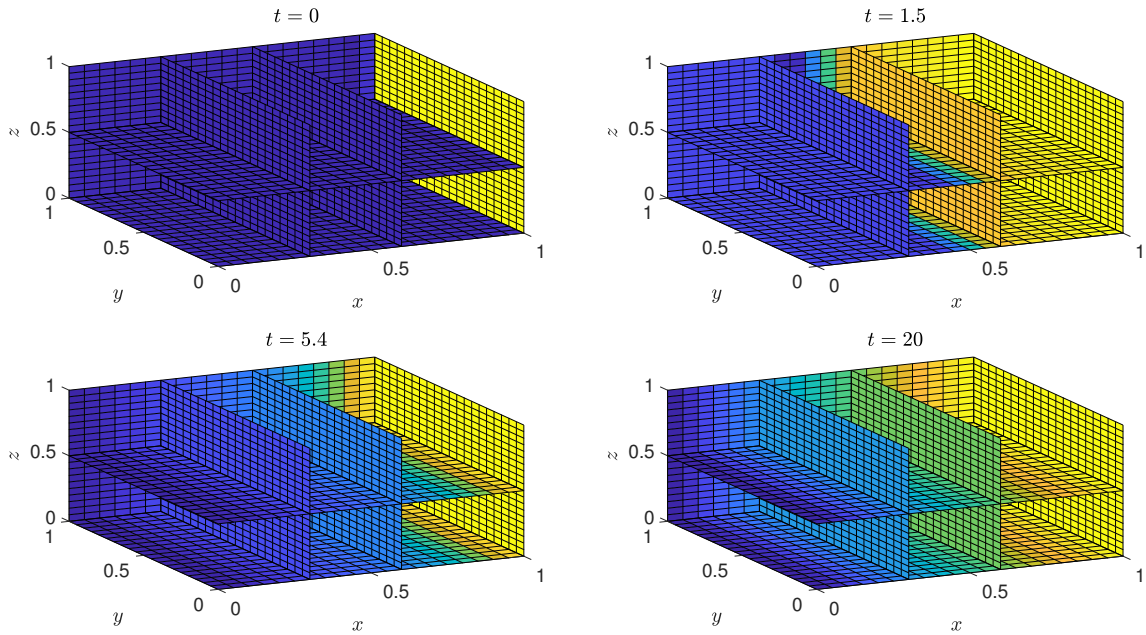


Figure 12: Snapshots of the solution to the hyperbolic heat equation in three dimensions with two opposing thermostatted walls, and the remaining walls thermally insulated.

5. 3D Simulations

In three dimensions, each cubic section of the domain was partitioned into tetrahedra as illustrated in figure 11. The three different figures show three different types of tetrahedra, occurring in pairs in each cubic section. Separate sets of basis functions were constructed for each type of tetrahedron. The method was tested on cases equivalent to the lower-dimensional cases. For the case of two opposing thermostats with the remaining walls insulated, snapshots are given in figure 12. For the case of only one thermostat, they are given in figure 13.

The results in three dimensions are again completely analogous to the lower dimensional results. The thermostatted cases have translational invariance in the $y - z$ -plane, and the solutions therefore act like planes of one-dimensional solutions. In particular, for the case in figure 12 which has a very long relaxation time τ , the wave front travelling towards $x = 0$ is quickly reflected and gives a cooling wave front which hits the $x = 1$ -plane shortly after, before the solution finally starts relaxing towards the stationary state.

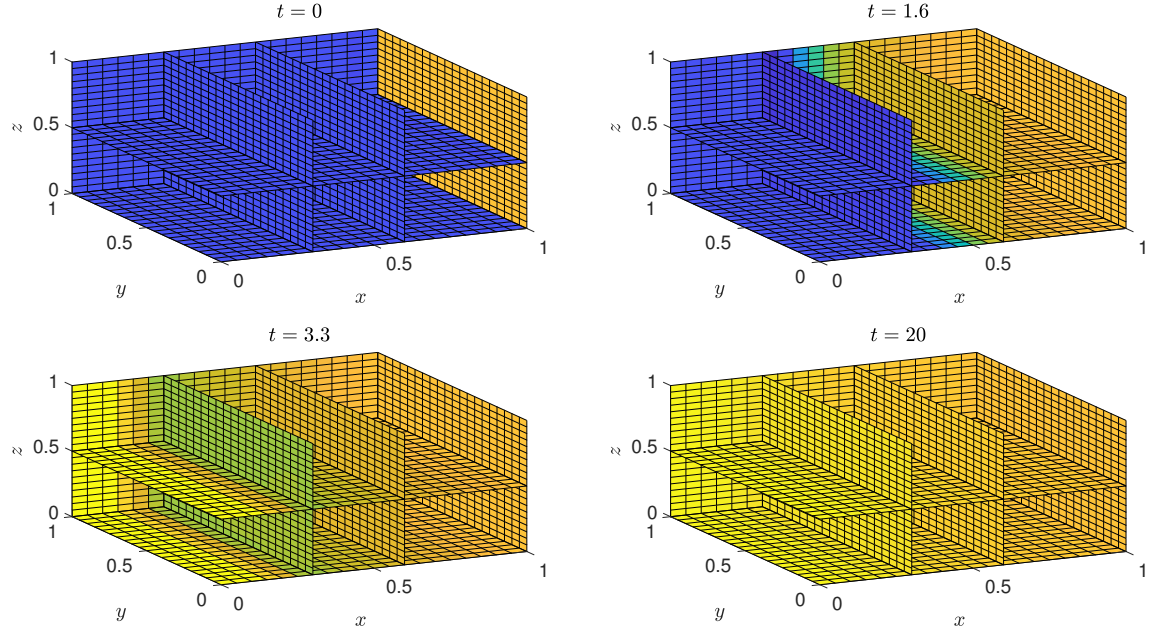


Figure 13: Snapshots of the solution to the hyperbolic heat equation in three dimensions with one thermostatted wall, and the remaining walls thermally insulated.

6. Concluding Remarks

The results obtained in this project illustrate how heat conduction on short timescales compared to typical system length scales compare to the classical Fourier type heat conduction. The hyperbolic variant of the heat equation puts an upper limit on the speed of information propagation in the system, which is a constraint required by special relativity. As non-equilibrium molecular dynamics simulations approach the investigation of dynamical systems on very short time scales, methods such as the finite element method can be useful tools for comparing results, as solving such macroscopic differential equations is generally much cheaper than calculating the detailed particle dynamics. It can also be helpful in investigating how variation of simulation parameters can be expected to affect the behavior of the system, without resorting to actually trying out several possibilities in expensive molecular dynamics simulations.

References

- [1] A. Quarteroni, *Numerical Models for Differential Problems*, 2nd Edition. Springer, 2013.